PI3K inhibitors synergize with FGFR inhibitors to enhance antitumor responses in FGFR2-mutant endometrial cancers

Leisl M. Packer[1*], Xinyan Geng[1*], Vanessa F. Bonazzi[1], Robert Ju[1], Clare Mahon[1], Margaret C. Cummings[2], Sally-Anne Stephenson[3], Pamela M. Pollock[1]

[1]Endometrial Cancer Laboratory, Queensland University of Technology (QUT) located within the Translational Research Institute, Queensland, Australia.
[2]School of Medicine, University of Queensland Centre for Clinical Research, Queensland, Australia.
[3]Eph Receptor Biology Group, Queensland University of Technology (QUT) located within the Translational Research Institute, Queensland, Australia.

***These authors contributed equally to this work.**

Running title.
FGFR and PI3K inhibitors in FGFR2^{mutant} endometrial cancer.

Keywords.
Endometrial cancer, FGFR2 mutation, BGJ398, GDC-0941, BKM120, BYL719, synergy

Conflict of Interest.
Dr Pollock is an inventor of two patents involving the detection of FGFR2 mutations for diagnostic or prognostic purposes in endometrial cancer. The remaining authors declare no conflicts of interests.

Financial support.
LP has been supported by NHMRC CJ Martin Fellowship (443038). PMP has been supported by an NHMRC CDF2 Fellowship (#1032851). Work is supported by a Cancer Australia Grant (#1087165).

* Corresponding author

Pamela M. Pollock

Institute of Health and Biomedical Innovation,
School of Biomedical Science,
Queensland University of Technology at the Translational Research Institute,
37 Kent Road
Woolloongabba QLD
AUSTRALIA 4059
Ph: +61 7 3443 7237

Email: pamela.pollock@qut.edu.au

Abstract

Improved therapeutic approaches are needed for the treatment of recurrent and metastatic endometrial cancer (EC). ECs display hyper-activation of the MAPK and PI3K pathways, the result of somatic aberrations in genes such as *FGFR2*, *KRAS*, *PTEN*, *PIK3CA* and *PIK3R1*. FGFR2, as well as the PI3K pathway, have emerged as potential therapeutic targets in EC. Activation of the PI3K pathway is seen in >90% of FGFR2^{mutant} ECs. This study aimed to examine the efficacy of the pan-FGFR inhibitor BGJ398 with pan-PI3K inhibitors (GDC-0941, BKM120) and the p110α-selective inhibitor BYL719. We assessed synergy in three FGFR2^{mutant} EC cell lines (AN3CA, JHUEM2 and MFE296) and the combination of BGJ398 and GDC-0941 or BYL719 showed strong synergy. A significant increase in cell death and decrease in long-term survival was seen when PI3K inhibitors were combined with BGJ398. Importantly, these effects were seen at low concentrations correlating to only partial inhibition of AKT. The combination of BGJ398 and GDC-0941 showed tumor regressions *in vivo,* whereas each drug alone only showed moderate tumor growth inhibition. BYL719 alone resulted in increased tumor growth of AN3CA xenografts, but in combination with BGJ398 resulted in tumor regression in both AN3CA and JHUEM2-derived xenografts. These data provide evidence that sub-therapeutic doses of PI3K inhibitors enhance the efficacy of anti-FGFR therapies and a combination therapy may represent a superior therapeutic treatment in FGFR2^{mutant} EC patients.

Introduction

Endometrial cancer (EC) is the most common gynaecological malignancy in developed countries and its incidence is increasing in postmenopausal women (1). In 2016 the American Cancer Society estimates that ~10,500 USA women will die of EC (2). Treatment options for patients with recurrent or persistent EC are limited to radiation and chemotherapy, which offer limited clinical benefit. As a result, the average survival of patients with metastatic or recurrent EC is only 7-12 months (3). Thus, there is a need for more effective therapies with reduced side effects, as well as predictive biomarkers to identify patients most likely to respond to these treatment options.

Our group and others have identified activating somatic mutations in *FGFR2* in ~10% of patients presenting with primary endometrioid EC (4-9). With regards to the EC subtypes identified by The Cancer Genome Atlas (TCGA), FGFR2 mutations occur at similar frequency in the microsatellite instability (MSI) hypermutated subtype as well as the copy number low subtype, which has also been described as those tumors with no specific molecular aberration (NSMP)(7,10). More recently, mutational analysis in a large multi-institute cohort has revealed FGFR2 mutations are more common in the tumors of patients that present with late stage disease (17%) as well as those that progress (progressed, recurred or died from disease) (26%) (11). In multivariate analysis where age, grade and stage were also taken into account, the presence of an *FGFR2* mutation was associated with decreased progression-free survival and decreased EC- specific survival (11).

Preclinical studies by our group and others have shown that *FGFR2*^{mutant} EC cells are highly sensitive to a range of FGFR inhibitors including PD173074 (5,12) ponatinib (13,14), BGJ398, dovitinib (15) and AZD4547 (16). The majority (93%) of *FGFR2*^{mutant} ECs also harbor mutations in the PI3K pathway (*PIK3CA*, *PIK3CB*, *PIK3R1*, *PIK3R2*, *PTEN*, *AKT1*) (7). Western blot analyses of *FGFR2*^{mutant} EC cell lines show that FGFR inhibitors fail to completely block PI3K pathway activation (12,15,16). Although these *in vitro* studies had shown classic oncogene addiction in *FGFR2*^{mutant} EC cell lines, *in vivo* studies with 30 mg/kg BGJ398 showed FGFR inhibition alone in the *FGFR2*^{mutant} AN3CA cell line lead to a delay in tumor growth but not

tumor regression (15). More recently, a similar study evaluating 30 mg/kg AZD4547 in AN3CA xenografts *in vivo* did show tumor regression (16), consistent with earlier studies performed in our lab using twice daily dosing of PD173074 (data not shown).

The PI3K pathway regulates proteins involved in cell cycle, survival and metabolism. It is thought to be the most commonly activated signaling pathway in human cancer and EECs have amongst the highest frequency (80-90%) of somatic mutations affecting this pathway (7,8). In most tumor types loss of PTEN and activation of PIK3CA are mutually exclusive events, however EC is unusual in that many tumors carry aberrations in multiple members of this signaling pathway (7).

There are several different classes of PI3K pathway inhibitors designed to target this pathway at one or more nodes and these include pan-PI3K, isoform-specific PI3K, mTOR, AKT, dual PI3K/mTOR and dual mTORC1/mTORC2 inhibitors (reviewed in 17). Unfortunately, many inhibitors targeting this pathway have shown disappointing results in Phase II/III clinical trials, and this has been attributed to a small therapeutic window accompanied by on-target toxicity from inhibiting this pathway in normal tissues, as well as a lack of predictive biomarkers to better identify the patients that will respond (18,19).

In this study we chose to evaluate BGJ398 (Infigratinib), an orally bioavailable selective pan-FGFR inhibitor currently being evaluated in Phase II trials as a single agent in several FGFR-dependent malignancies (NCT02160041, NCT02150967) as well as the pan-PI3K inhibitor (BKM120) and the p110α-selective inhibitor BYL719 (Alpelisib), all developed by Novartis. Of direct relevance to this project, there is currently a Phase Ib expansion trial evaluating the efficacy of BGJ398 + BYL719 in breast and lung cancers (NCT01928459). As BKM120 has been shown to possess off-target effects at concentrations above 1 μM (20), we also assessed BGJ398 in combination with the class I pan-PI3K inhibitor GDC-0941 (Pictilisib). This research shows that partial abrogation of signaling through the PI3K pathway enhances the efficacy of BGJ398 in *FGFR2*^{mutant} EC models *in vitro* and *in vivo*.

Material and Methods

Cell lines, Culture conditions and Inhibitors

AN3CA, MFE296 and JHUEM2 were obtained from ATCC (2005), ECACC (2007) and Riken Cell Bank (2012) respectively. AN3CA, JHUEM2 and MFE296 were authenticated by STR profiling at sequencing facility of The QIMR Berghofer Medical Research Institute in 2013 and 2016 and passaged less than 20 times since authentication. AN3CA and MFE296 cells were grown in MEM-alpha and JHUEM2 cells in 1:1 DMEM:HamF12, supplemented with 10% fetal bovine serum, 1% penicillin/streptomycin and 0.1 mM non-essential amino acids. According to the Cancer Cell Line Encyclopedia, the cell lines harbor the following mutations; AN3CA express FGFR2 N550K and K310R, PIK3R1 p.557_561REIDK>Q and PTEN p.R130fs; JHUEM2 express FGFR2 C383R, PIK3CA p.V344G, p.E978K, PIK3R1 p.N707del and PTEN p.N212_splice; MFE296 cells harbor FGFR2 N550K, PIK3CA p.I20M, p.P539R and PTEN p.R130Q and p.T321fs*23. Kinase inhibitors (BGJ398, GDC-0941, BKM120 and BYL719) were purchased from Selleck Chemicals for *in vitro* experiments and from Synkinase for *in vivo* studies. Structures of compounds are shown in Figure S1B.

Cell Viability Assay

Cell viability was assessed by sulforhodamine B staining. Briefly, 3000 cells were seeded in a 96-well plate. The following day cells were treated with half-log dilutions of drug (1 nM to 10 μM). After 96 hours, cells were fixed in methanol, stained with SRB, solubilized with 10 mM Tris and absorbance read at 492 nm. Values were normalized to DMSO control. IC_{50} values are the mean of three independent experiments and were calculated using nonlinear regression analysis with variable slope in GraphPad Prism v6.0.

Chou-Talalay Drug Combination Study

Synergy between BGJ398 and the PI3K inhibitors was assessed using the methodology proposed by Chou and Talalay (21). Drug concentrations were in a series of 2-fold dilutions

above and below the IC_{50} of each drug. One day after seeding, cells were treated with BGJ398, GDC-0941, BYL719, BKM120 alone or in combination for 96 hours. All experiments were repeated three independent times. The combination index and fraction affected was calculated by Calcusyn, v2.0 (Biosoft).

Colony Forming Assay

Cells (600-1000) were seeded in 6-well plates and the following day treated with DMSO or inhibitors for 72 hours. Cells were washed thrice in PBS and grown in full-growth medium for 10-16 days, fixed with methanol and stained with crystal violet (0.1% in 25% methanol). Colonies were counted and the mean of 2 (JHUEM2) or 3 (AN3CA, MFE296) independent experiments (each performed in triplicate) was plotted as a percentage of the DMSO control.

Assessment of apoptosis

Cells (4×10^5) were seeded in 6-well plates overnight. On the second day, cells were treated with the indicated drugs or DMSO for 72 hours. Floating and attached cells were collected and analyzed for Annexin and PI staining according to the manufacturer's instructions (FITC Annexin V Apoptosis Detection Kit II, BD Biosciences) using BD LSR II and Flowjo, v10.7.

siRNA-mediated depletion of p110α and p110β

AN3CA and JHUEM2 cells ($3.5x10^5$) were reversed-transfected with 10nmol Dharmacon ON-TARGETplus siRNA pools targeting p110α/PIK3CA and p110β/PIK3CB or a non-targeting control (D-001810-10) using Lipofectamine RNAiMAX in serum-free media in a 6-well plate. Full-growth media was added 24 hours. Fourty-eight hours post–transfection, cells were treated with DMSO, 0.3 μM GDC-0941 or 0.6 μM BYL719 for 6 hours then lysed and subjected to Western blot analysis. Quantification of band intensities from duplicate (JHUEM2) and triplicate (AN3CA) experiments (normalized to tubulin) was performed using ImageJ.

Immunoprecipitation, Western blot analysis and antibodies

Proteins were harvested using RIPA buffer (50 mM Tris pH 7.4, 150 mM NaCl, 1 mM EDTA, 1% IGEPAL, 0.1% SDS, 0.5% sodium deoxycholate, 1 mM sodium orthovanadate, 1 mM NaF, 1 mM PMSF, 10 μg/ml aprotinin and leupeptin). For immunoprecipitation, 1 mg of protein lysate was pre-cleared with Protein A SureBeads beads (Bio-Rad) for 30 min prior to incubating the lysate with anti-FGFR2 (C-17) antibody (Santa Cruz) and Protein A SureBeads beads overnight at 4°C. Western blotting was performed using standard protocols. The following antibodies were used: p110α (#4249), p110β (#3011), PARP (#9542), pFRS2α(Tyr436) (#3861), pAKT(Ser473) (#4060), AKT (#2920), pERK(Thr202/Tyr204) (#4695), ERK (#9107), pS6 (Ser240/244) (#2215), S6 (#2317), p-Tyr-100 (#9411) from Cell Signaling Technology; pERK (Thr202/Tyr204) (mouse), Tubulin (T9026) from Sigma; FGFR2 Bek-C17 (sc-122), ERK2 (sc-154), FRS2 (sc-8318) and GAPDH (sc-32233) antibodies from Santa Cruz Biotechnology, Inc. Secondary antibodies IRDye 680LT Donkey anti-Rabbit IgG (C31024-04) and IRDye 800CW Donkey anti-mouse IgG (#C30904-02) were from LI-COR® Corporate.

***In vivo* murine xenograft model**

Six-week-old female NOD-SCID mice (15-18 g) were purchased from the Animal Resources Centre (Canningvale, WA, Australia) and hosted in the pathogen-free Biological Resource Facility (BRF) of the Translational Research Institute, Brisbane, Australia. Mice were maintained and handled under aseptic conditions, and were allowed access to food and water *ad libitum*. *In vivo* animal studies were performed according to institution-approved protocols (TRI/160/14/AUC) and guidelines for maintenance of animals and end point of tumor studies were followed. Xenografts of AN3CA and JHUEM2 EC cell lines were established by subcutaneously injecting 1×10^6 viable cells in growth factor-reduced matrigel (#354230, BD Biosciences) 1:1 with PBS into the flank of the mice. Perpendicular tumor diameters were measured by a single observer

using Vernier scale calipers, and tumor volumes were calculated using the formula [($x \times y^2$)/2]. JHUEM2 and AN3CA xenografts were allowed to grow for 10 and 14 days respectively (to allow formation of tumors with mean xenograft volume ~150mm^3). Mice were then stratified into treatment groups with one tumor per mouse on the basis of their weight and tumor volume. Mice (8/group) were treated for three weeks *via* oral gavage, 5 days on/1 day off, of (i) vehicle control (100 mM acetic acid/sodium acetate buffer pH 4.6/PEG300 (1:1)), (ii) BGJ398, 20 mg/kg, (iii) GDC-0941, 75 mg/kg, (iv) BYL719, 12.5 mg/kg, (v) BGJ398 + GDC-0941 and (vi) BGJ398 + BYL719. Body weight was recorded for each animal every other day to monitor potential toxicities. Additional animals (4/group) were treated for 4 days, with their final treatment 6 hours prior to tumor collection. Part of the tumor was snap-frozen, then lysed in RIPA lysis buffer (2.5 µl/mg) for Western blot analysis and the other part fixed in 4% paraformaldehyde.

Immunohistochemical staining of mouse xenografts

Tumors were fixed in 4% paraformaldehyde solution overnight, paraffin-embedded and cut into 5 µm-thick sections. Sections were deparaffinized, rehydrated, followed by antigen retrieval with CC1 buffer at 100 ^{o}C for 64 mins using the Ventana Discovery Ultra. Slides were blocked with Discovery Inhibitor for 8 mins, incubated with Anti-Rabbit Cleaved Caspase-3 antibody (#9661; Cell Signaling Technology) for one hour at 37^{o}C, followed by secondary anti-Rabbit HQ and anti-HQ HRP. The signal was detected with DAB substrate (Discovery ChomoMap kit) followed by a haemotoxylin counterstain. All images were taken with Olympus IX73 inverted Fluorescence microscope fitted with XM10 monochrome camera. Histopathologic scoring of cleaved caspase 3 was performed on five fields (x400 magnification) for each of the four tumors treated with the different drug/s avoiding areas of marked necrosis. Identification of positive cells was performed blinded and independently on a multi-header microscope by MC, VB and PP and averaged for each sample and condition. Data for caspase positivity for each drug treatment is presented as a ratio over vehicle control.

Statistical Analysis

The *in vitro* data was analyzed using one-way ANOVA with Tukey's multiple comparison to test all treatment combinations. Differences in xenograft volume between groups were assessed for significance using a repeated two-way ANOVA. *p*-values, calculated with Prism (Graphpad), are coded by asterisks: <0.05 (*), <0.01 (**), <0.001 (***), *P*<0.0001(****).

Results

Effects of BGJ398, GDC-0941, BKM120 and BYL719 on ERK and AKT activity

We first determined the effect of increasing concentrations of BGJ398, GDC-0941, BKM120 and BYL719 on phospho-ERK (pERK) and phopsho-AKT (pAKT) downstream signaling in FGFR2^{mutant} EC cell lines AN3CA and JHUEM2. Both AN3CA and JHUEM2 cells showed complete inhibition of ERK activity at 0.1 μM BGJ398 (Figure S1A). While phosphorylated ERK1/2 is often used to indicate FGFR inhibition, we confirmed inhibition of FGFR2 by BGJ398 by immunoprecipitating FGFR2 and staining for phosphorylated-tyrosine (Figure S1C). As expected, BGJ398 caused loss of phosphorylated FGFR2 in all three cell lines. AKT (Ser473) phosphorylation was unchanged even at higher concentrations of BGJ398. This is consistent with previous data we have published using the FGFR inhibitor PD173074 (12). The pan-PI3K inhibitor GDC-0941 showed significant inhibition of AKT activity in JHUEM2 and AN3CA at 0.3 μM and complete inhibition at 1 μM, whereas higher concentrations of BKM120 were required to obtain similar pathway inhibition (Figure S1). JHUEM2 cells were more sensitive to the p110α/PIK3CA-specific inhibitor BYL719, consistent with this cell line carrying activating mutations in *PIK3CA*.

BGJ398 synergizes with PI3K inhibition to inhibit cell proliferation

In order to assess synergy, the half maximal inhibitory concentration (IC_{50}) for each single agent (BGJ398, GDC-0941, BKM120 and BYL719) was determined (Table 1). AN3CA and JHUEM2 were slightly more sensitive to BGJ398 (IC_{50} 20 nM and 30 nM, respectively) than MFE296 (IC_{50} 80 nM). AN3CA cells showed greater sensitivity to GDC-0941 than JHUEM2 and MFE296 cells, with an IC_{50} value of 140 nM compared to 355 nM and 630 nM respectively. JHUEM2 cells were more sensitive to BYL719, with an IC_{50} value of 530 nM compared to 1730 nM for AN3CA and 4050 nM for MFE296. AN3CA and JHUEM2 cells responded in a similar manner to BKM120, with IC_{50} values of 320 nM and 260 nM respectively.

These IC_{50} values were used to assess potential synergy using the Chou-Talalay equipotent

fixed ratio method (Figure 1A- I). Combination treatment of AN3CA, JHUEM2 and MFE296 cells with BGJ398 and either GDC-0941 or BYL719 resulted in enhanced inhibition of cell proliferation compared to BGJ398 alone. The combination of BGJ398 with GDC-0941 or BYL719 was synergistic (combination index values < 0.7) at all concentrations in JHUEM2 and MFE296 and in all but the lower two concentrations in AN3CA (Figure 1C, F, I). The BGJ398 and BKM120 combination had a more subtle effect, with synergy seen only at the highest concentrations (Figure S1D-F). These results suggest that dual treatment with BGJ398 and either GDC-0941 or BYL719 is more synergistic at inhibiting proliferation of FGFR2^{mutant} EC cells than BGJ398 combined with BKM120.

Co-targeting FGFR2 and PI3K signaling reduces long-term cell survival

Clonogenic assays were performed to further examine the effect of the combination treatments on long-term cell survival and to determine if synergy could be seen at clinically relevant doses (Figure 2). Plasma concentrations of BGJ398 in phase I trial patients were found to have a C_{min}-C_{max} range of approximately 100-450 nM (22) and as such 100 nM and 300 nM concentrations were assessed, as these represented a low and mid range concentration, respectively. The reported C_{max} of GDC-0941, BYL719 and BKM120 is 2.07 μM (23), 2.3 μM (24) and 1.8 μM (25) respectively, therefore 0.3, 0.6 and 1 μM were initially assessed. When combined with BGJ398, even low concentrations of the PI3K inhibitors caused a substantial reduction in colony formation (Figure S2A-B), despite the small reduction in AKT phosphorylation seen with the lower drug concentrations (Figure S1). For subsequent analysis, we used 0.3 μM GDC-0941, 0.6 μM BYL719 and 0.6 μM BKM120. These concentrations were well below the plasma C_{max} values (often close to the C_{min}) such that evidence of synergism might open new avenues for using these drugs at sub-therapeutic doses.

Treatment with 0.3 μM BGJ398 significantly reduced colony formation by ~70% (P< 0.0001) in AN3CA cells (Figure 2A, B). Long-term survival of AN3CA cells was slightly reduced by single agent PI3K inhibitor treatment, suggesting this pathway contributes to the survival of

these cells. GDC-0941 alone significantly reduced colony formation by ~50% (P<0.0001), whereas BYL719 and BKM120 only reduced colony formation by 20% and ~35% (P<0.01) respectively. In AN3CA cells, combining BGJ398 with GDC-0941, BYL719 or BKM120 reduced clonogenic survival by a further 20-30% compared to BGJ398 single agent treatment (BGJ + GDC P<0.01, BGJ + BYL P<0.05, one way ANOVA). In JHUEM2 cells, BGJ398 treatment led to a ~50% reduction (P<0.001) in colony formation, whereas single agent PI3K inhibition had no significant effect (Figure 2C, D). Nevertheless these cells were particularly sensitive to dual inhibition of FGFR2 and PI3K, with a further reduction of ~40-50% (P<0.01) by all three PI3K inhibitors compared to BGJ398 treatment alone. The colony formation in MFE296 cells was significantly reduced by BGJ398 (~75% reduction; p>0.0001), but not by any of the PI3K inhibitors alone. The combination of GDC-0941 or BKM120 with BGJ398 further reduced the colony formation by 15% (ns) and 10% (ns) respectively, but no additional benefit was seen when BYL719 was combined with BGJ398. It should be noted that for this assay, cells were treated with single agents or combinations for 72 hours after which cells were washed to remove residual drugs before plating, so this assay under-represents the cell death that would be seen following continuous drug exposure.

BGJ398 synergizes with PI3K inhibition to induce cell death

To test the hypothesis that BGJ398 combined with a PI3K inhibitor enhances apoptosis, Annexin V positivity was assessed following 72 hours drug treatment (Figure 2E). Treatment with BGJ398 alone induced approximately 30% - 40% cell death in AN3CA (P<0.05), JHUEM2 (P<0.0001) and MFE296 (P<0.05), compared to 10% in the vehicle control (Figure 2G-I). The single agent PI3K inhibitors had little effect on cell death in any cell line at the low concentrations chosen. The combination of BGJ398 with any of the PI3K inhibitors induced significantly more cell death than BGJ398 alone. This data demonstrate that combining the FGFR inhibitor BGJ398 with a pan-PI3K or p110α/PIK3CA-selective inhibitor not only reduces cell proliferation and long-term survival, but also enhances the effect of BGJ398 in inducing cell death in BGJ398-

sensitive EC cells.

The combination of BGJ398 and a PI3K inhibitor caused enhanced inhibition of AKT and downstream target S6

To understand the molecular basis of the synergistic cell death induced by the combination of BGJ398 and PI3K inhibitors we measured the response of key downstream targets to the individual inhibitors and combinatorial treatments after 1, 8 and 24 hours (Figure 3A, 3B, S3). Phosphorylation of ERK, a downstream marker of FGFR activity, is totally abrogated by 0.3 μM BGJ398 at all time points in all three cell lines. BGJ398 slightly blocks AKT phosphorylation in JHUEM2 and MFE296 and shows little effect on AKT phosphorylation in AN3CA cells.

In JHUEM2 all three PI3K inhibitors inhibit AKT activity to a similar extent, leading to dephosphorylation of S6 at 8 and 24 hours. In AN3CA and MFE296 cells, GDC-0941 is the most effective inhibitor of AKT and S6 with strongest inhibition seen at the earlier two timepoints. BYL719 has little effect on AKT or S6 activity in AN3CA cells. This may be explained by the lack of a *PIK3CA* mutation in AN3CA cells, the presence of which likely sensitizes JHUEM2 cells to this isoform-selective inhibitor. The inhibition of the PI3K pathway by single agents is short-lived, with phospho-S6 levels returning to almost normal by 24 hours in AN3CA and JHUEM2. The dephosphorylation of S6 in response to dual targeting of the FGFR and PI3K pathways was greatest at 8 hours and still evident at 24 hours in all three cell lines.

Preferential signaling of JHUEM2 cells through p110α/PIK3CA

To determine whether AN3CA and JHUEM2 cells show preferential signaling through p110α/PIK3CA or p110β/PIK3CB, siRNA knockdown of each gene was performed (Figure 3C). As predicted, knockdown of p110α in JHUEM2 (*PIK3CA*^{mutant}) resulted in almost complete inhibition AKT and S6, suggesting that p110α regulates PI3K pathway activity in these cells. In contrast, while p110α knockdown in AN3CA (*PIK3CA*^{WT}) cells inhibited AKT (though to a lesser extent than

JHUEM2), this did not translate into an equivalent inhibition of the downstream effector S6, suggesting that AN3CA does not solely rely on p110α/PIK3CA for PI3K pathway activation.

Knockdown of p110β resulted in an unexpected increase in the expression of p110α in both cell line models (Figure 3D), which resulted in an increase in the activation of AKT and S6 (Figure 3C), unlike knockdown of p110α, which did not alter p110β levels (Figure 3D). Knockdown of both p110α and p110β abrogated this activation of AKT signaling. The pan-PI3K inhibitor GDC-0941 almost completely inhibits AKT/S6 signaling in AN3CA, more so than the combined siRNAs (which elicit only partial knockdown), suggesting that AN3CA relies on both p110α and p110β for PI3K pathway activation.

Combined BGJ398 and PI3K inhibition induced marked tumor regression in FGFR2^{mutant} xenograft models *in vivo*

We then studied the anti-tumor activity of the BGJ398 + GDC-0941 and BGJ398 + BYL719 combinations in AN3CA- and JHUEM2-derived murine xenografts. BGJ398, GDC-0941 and BYL719 alone and in combination were well tolerated with no significant weight loss observed throughout the course of treatment (Figure S4A, B). While BGJ398 has been used at concentrations ranging from 5 mg/kg to 45 mg/kg *in vivo* (26), we utilized a concentration of 20 mg/kg in order to detect increased efficacy in our combination studies. As expected, 20 mg/kg BGJ398 resulted in significantly delayed tumor growth in both cell line models compared with the control group (P<0.001, Figure 4A, 4B). GDC-0941 (75 mg/kg) and BYL719 (12.5 mg/kg) administered as single agents had surprising opposite effects. GDC-0941 inhibited tumor growth to a similar extent as BGJ398, consistent with increased pathway inhibition by 75 mg/kg GDC-0941 *in vivo* compared to the lower concentrations utilized for the *in vitro* studies (Figure 4D). In contrast, BYL719 monotherapy unexpectedly enhanced the growth of AN3CA-derived tumors (P<0.0001).

Combinatory treatment of BGJ398 + GDC-0941 and BGJ398 + BYL719 resulted in a marked inhibition of tumor growth in both AN3CA (P<0.001, P<0.05 respectively) and JHUEM2

xenograft models, compared to the BGJ398-treated groups. Indeed, these combinations caused complete or partial tumor regression, with no palpable tumor present in 5/8 and 4/8 mice with AN3CA and 2/8 and 1/8 mice with JHUEM xenografts treated with BGJ398 + GDC-0941 and BGJ398 + BYL719 respectively (Figure S4B).

Biochemically, BGJ398-treated xenografts show partial inhibition of AKT and almost complete inhibition of ERK at 4 days (Figure 4D). AN3CA xenografts treated with GDC-0941 for 4 days show marked reduction in pAKT, pS6 and p4EBP-1 levels, confirming inhibition of the PI3K pathway. BYL719 treatment also resulted in a reduction in pAKT and pS6 levels, albeit not to the extent seen with GDC-0941. The combination of BGJ398 + GDC-0941 caused a stronger reduction in pAKT, pS6 and p4EBP1 than GDC-0941 alone. These results are consistent with the cell death and clonogenic data, which confirm that a synergistic effect occurs when blocking FGFR and PI3K pathways.

Histological analysis of the AN3CA tumors, which had been treated for four days, revealed very frequent mitoses in both the vehicle control and in the BYL719 tumors (data not shown). Only occasional apoptotic bodies were observed in the GDC-0941 treated tumors whereas a high number of apoptotic bodies were seen in the tumors treated with BGJ398 + GDC-0941 (data not shown). Both combination treatments showed broad, confluent areas of necrosis.

Assessment of cell death markers following dual targeting of FGFR and PI3K pathways

The single agent and combination treatments were assessed for their effect on the apoptotic marker PARP and cleaved caspase 3 (Figure 3A, 3B and 4E). In AN3CA cells, cleavage of PARP resulting in 25 and 89 kDa fragments, is more pronounced following treatment with BGJ398 + GDC-0941 at 8 and 24 hours (Figure 3A). This is consistent with a significant increase in caspase 3 cleavage by the BGJ398 + GDC-0941 combination in AN3CA-derived xenografts and the presence of numerous apoptotic bodies compared to BGJ398 and GDC-0941 single treatments (Figure 4E). This high level of caspase cleavage is not observed with the BGJ398 + BYL719 combination in the

AN3CA xenografts, despite large areas of tumor necrosis evident histologically, suggesting different mechanisms of cell death may be occurring.

Similar annexin positivity was seen with all three combinations (Figure 2G), suggesting that BYL719 and BKM120 might elicit a different cell death mechanism. The inhibition of AKT caused by BYL719 alone or in combination with BGJ398 is much less than that caused by GDC-0941. It is possible that only minor abrogation of AKT signaling is required to kill AN3CA cells when FGFR is also inhibited. In contrast to the results observed in AN3CA cells, a strong induction of PARP cleavage in response to BGJ398 was seen in JHUEM2 cells, which was enhanced equally in all three PI3K inhibitor combinations treatments. This PARP cleavage coincides with similar levels of Annexin V positivity seen at 72 hours in all three combinations (Figure 2H).

Discussion

Small molecule inhibitors that target oncogenic drivers of tumorigenesis are becoming standard therapies in many cancer types. Given the high frequency of PI3K aberrations in EC, several Phase II trials evaluating PI3K inhibitors as single agents have been undertaken, with overall disappointing results (27). A number of FGFR inhibitors have shown remarkable clinical responses in a subset of other FGFR dependent malignancies (28,29), but to date only multi-kinase inhibitors such as dovitinib have been tested in EC (30). No complete responses were documented in the latter, however no hyperphosphatemia was reported, bringing into question whether sufficient inhibition of the FGFR receptors was obtained. Although FGFR inhibitors have been shown to induce cell death in FGFR2^{mutant} EC cell lines with concomitant PI3K pathway activation (12), it is reasonable to assume that the co-occurrence of activating PI3K pathway mutations may limit the extent and durability of tumor responses to single agent FGFR inhibitors.

Here we show that multiple inhibitors targeting the PI3K pathway enhance the efficacy of the FGFR inhibitor BGJ398 in FGFR2^{mutant} ECs. Notably, we show that low doses of PI3K inhibitors, correlating with only partial inhibition of AKT phosphorylation, synergize with FGFR inhibition to achieve cell death and tumor shrinkage *in vivo*. Our data suggests isoform-specific inhibition of p110α by BYL719 has different effects in AN3CA and JHUEM2 cells. In JHUEM2 cells, carrying an activating *PIK3CA* mutation, BYL719 resulted in partial AKT inhibition, a small decrease in pS6 phosphorylation (Figure 3B) and a slowing of tumor growth *in vivo* (Figure 4B). In AN3CA cells, BYL719 had less of an effect on pAKT (Figure 3A and 5A), with little to no reduction of phosphorylated pS6, suggesting that inhibition of the PI3K/AKT/mTORC1 pathway by this p110α-specific inhibitor is incomplete. Unexpectedly BYL719 single agent treatment increased growth of AN3CA-derived xenografts (Figure 3A), which is blocked by the addition of BGJ398. This suggests that whatever pro-survival pathway is being activated by BYL719 in AN3CA tumors, it is blocked by pan-FGFR inhibition.

Activation of parallel pathways have previously been implicated in resistance to PI3K inhibitors (reviewed in 31), leading to the belief that combination therapies are required to overcome such feedback loops. Further studies are required to understand the molecular basis of BYL719-induced tumor growth in AN3CA xenografts.

The differential reliance of AN3CA and JHUEM2 on p110α/PIK3CA may explain their differential response to BYL719. BYL719 inhibits AKT/S6 signaling to a greater extent in JHUEM2 cells, resulting in PARP cleavage when combined with BGJ398 in JHUEM2 cells (Figure 3B), which are more reliant on p110α than AN3CA (Figure 3C). In contrast, PI3K signaling is only partially inhibited by BYL719 in AN3CA cells, which fails to cause PARP cleavage (Figure 3A) or caspase-dependent cell death in combination with BGJ398 (Figure 4E). These results suggest that complete PI3K inhibition is required to induce caspase-dependent cell death. The fact that BGJ398 + BYL719 induces tumor regression to the same extent as BGJ398 + GDC-0941 suggests that only partial inhibition of the PI3K pathway is needed to lower the apoptotic threshold of FGFR inhibitors. Furthermore, the results suggest that cell death induced by BYL719 is caspase-independent and may also be PI3K-independent.

Our results show that in the context of EC S6 is regulated by both the PI3K and FGFR2 pathways, with the combination treatments reducing levels of phosphorylated S6 more than the individual treatments (Figure 3). The sustained inhibition of S6 by combination treatment is likely the result of inhibiting both the PI3K and FGFR2 pathways. Together with previous studies targeting the PI3K pathway alone or in combination with MEK inhibition, these results indicate that levels of phosphorylated S6 may be an effective biomarker of response to targeting these key survival pathways (32-34).

Our data in EC is supported by similar combination studies in EC and other cancers. Specifically in EC, Gozgit *et al.* reported synergy between the multi-kinase inhibitor ponatinib and the mTOR inhibitor ridaforolimus (35). In liver cancer, the addition of the mTOR inhibitor RAD001 to dovitinib also showed an increase in growth inhibition of Hep3B xenografts (36) and the addition of the mTOR inhibitor rapamycin to BGJ398 resulted in increased tumor

growth inhibition in a subcutaneous and a syngeneic orthotopic model (37). In FGFR1-amplified lung cancer, the combination of BGJ398 and GDC-0941 led to enhanced growth suppression *in vivo* (38). Furthermore, a recent study in FGFR1-amplified lung and bladder cancer cells found that the FGFR inhibitor AZD4547 caused synergistic induction of cell death *in vitro* when combined with an mTOR inhibitor (either AZD8055 or KU0063794) or a pan-PI3K inhibitor (GDC-0941) (29).

Early trials using pan-PI3K inhibitors were associated with on-target toxicity. Thus, considerable effort has gone into developing PI3K isoform-selective inhibitors and the identification of predictive biomarkers for these isoform selective PI3K inhibitors. Initial studies utilizing both genetically engineered mouse models and panels of cell lines from multiple cancer types showed that PTEN-deficient breast and prostate cancer cells preferentially signal through p110β (39-41). Moreover, clinical resistance to BYL719 in a metastatic breast cancer lesion carrying an activating *PIK3CA* mutation was attributed to loss of PTEN in this specific lesion (42). More recently, there have been reports that PI3K isoform usage in the context of PTEN loss is dependent on the genetic context by which the PI3K pathway is activated. Tumors where the PI3K pathway was activated by either activated KRAS (43) or the polyoma middle T antigen (44) showed a reliance on p110α even in the presence of concurrent PTEN loss, in contrast to earlier studies where the reliance on p110β occurred only in models with PTEN loss.

Our attempt to determine whether preferential signaling through p110α or p110β was taking place in AN3CA or JHUEM2 cells was somewhat hindered by the unexpected activation of AKT following p110β depletion. While unexpected, our results were in line with those of Utermark and colleagues (45), showing that increased AKT activation in a conditional knockout of p110β in murine mammary epithelium in transgenic models of breast cancer driven by the polyoma middle T antigen or Her2/New resulted in enhanced tumor growth. The authors presented data indicating that there was competition between p110α and p110β for binding to the oncogenic receptor and removal of p110β allows increased binding of the more active p110α , leading to increased pathway activation (45). In

the endometrial cancer lines examined the increased AKT activation could be due to both an increase in p110α expression (Figure 3C, 3D) as well as higher activation of AKT elicited by p110α. Whether the ablation of p110β resulted in an increase in p110α expression was not assessed in the murine models, but the data presented here suggests a level of compensatory crosstalk that has not been previously reported.

As endometrial tumors are unique in that they often carry aberrations in multiple members of the PI3K pathway, identifying biomarkers of response to isoform-specific PI3K inhibitors in endometrial cancer has proven difficult. The study by Weigelt and colleagues investigating a number of drugs targeting different nodes of the PI3K pathway in a large panel of EC cell lines showed that PTEN-null ECs require inhibition of both p110α and p110β to reduce cell viability and suggest that the preferential use of specific catalytic subunits of PI3K may also depend on tissue context (17). This is in line with clinical data using mTOR inhibitors in EC where no association between specific mutations and clinical responses was observed (46). Our *in vitro* data is consistent with that of Weigelt *et al*. (17), with single agent pan-PI3K inhibitors GDC-0941 and BKM120 showing greater activity than BYL719 in a variety of assays. However, perhaps surprisingly, when combined with FGFR inhibition, p110α specific inhibition by BYL719 induced similar tumor growth inhibition to pan-PI3K inhibition with GDC-0941.

A variety of studies have demonstrated that crosstalk between the MAPK and PI3K signaling pathways are associated with resistance to targeted therapies (47-49). Thus, we hypothesize that dual inhibition of both the FGFR/MAPK axis and PI3K signaling pathways will not only induce more tumor cell death but also result in a decrease in intrinsic and acquired resistance. In a similar manner we would also hypothesize that pan-PI3K inhibition may well prevent the emergence of resistance *via* altered p110 isoform usage.

Although many companies are developing inhibitors against these pathways, only a few companies have inhibitors against both FGFR and the PI3K in clinical development. Arqule have a specific FGFR inhibitor (ARQ087) and a pan-AKT inhibitor (ARQ092/ARQ751) and Astra Zeneca

also have a pan-FGFR inhibitor (AZD4547) and a pan-AKT inhibitor (AKT5363). At this time Novartis have the only combination in clinical trials (BYL719 + BGJ398) with enrolment focused on those patients with an activating *PIK3CA* mutation. Our data, and that of Weigelt and colleagues (17), would suggest that pan-PI3K inhibition is more efficacious than isoform specific PIK3CA inhibition in EC. As with all combination therapies, there remains a need to determine whether the toxicities seen with inhibition of either the PI3K or FGFR pathways are additive or synergistic when blocked together. Our *in vitro* data suggests that sub-therapeutic inhibition of the PI3K pathway may be effective in combination, allowing lower doses and ideally less toxicity.

REFERENCES

1. Saso S, Chatterjee J, Georgiou E, Ditri AM, Smith JR, Ghaem-Maghami S. Endometrial cancer. BMJ **2011**;343:d3954
2. Society A. Cancer Facts & Figures 2016. Atlanta: American Cancer Society **2016**
3. Obel JC, Friberg G, Fleming GF. Chemotherapy in endometrial cancer. Clinical advances in Hematology & Oncology **2006**;4:459-68
4. Pollock PM, Gartside MG, Dejeza LC, Powell MA, Mallon MA, Davies H, et al. Frequent activating FGFR2 mutations in endometrial carcinomas parallel germline mutations associated with craniosynostosis and skeletal dysplasia syndromes. Oncogene **2007**;26:7158-62
5. Dutt A, Salvesen HB, Chen TH, Ramos AH, Onofrio RC, Hatton C, et al. Drug-sensitive FGFR2 mutations in endometrial carcinoma. Proc Natl Acad Sci U S A **2008**;105:8713-7
6. Byron SA, Gartside M, Powell MA, Wellens CL, Gao F, Mutch DG, et al. FGFR2 point mutations in 466 endometrioid endometrial tumors: relationship with MSI, KRAS, PIK3CA, CTNNB1 mutations and clinicopathological features. PloS One **2012**;7:e30801
7. Cancer Genome Atlas Research N, Kandoth C, Schultz N, Cherniack AD, Akbani R, Liu Y, et al. Integrated genomic characterization of endometrial carcinoma. Nature **2013**;497:67-73
8. Cheung L, Hennessy B, Li J, Yu S, Myers A, Djordjevic B. High frequency of PIK3R1 and PIK3R2 mutations in endometrial cancer elucidates a novel mechanism for regulation of PTEN protein stability. Cancer Discovery **2011**;1:170-85.
9. Krakstad C, Birkeland E, Seidel D, Kusonmano K, Petersen K, Mjos S, et al. High-throughput mutation profiling of primary and metastatic endometrial cancers identifies KRAS, FGFR2 and PIK3CA to be frequently mutated. PloS One **2012**;7:e52795.
10. Stelloo E, Nout RA, Osse EM, Jurgenliemk-Schulz IJ, Jobsen JJ, Lutgens LC, et al. Improved Risk Assessment by Integrating Molecular and Clinicopathological Factors in Early-stage Endometrial Cancer-Combined Analysis of the PORTEC Cohorts. Clinical Cancer Research **2016**;22:4215-24.
11. Jeske Y, Ali S, Byron S, Gao F, Mannel R, Ghebre R, et al. FGFR2 mutations are associated with poor outcomes in endometrioid endometrial cancer: An NRG Oncology/Gynecologic Oncology Group study. Submitted to Gynaecological Oncology **2016**
12. Byron SA, Gartside MG, Wellens CL, Mallon MA, Keenan JB, Powell MA, et al. Inhibition of activated fibroblast growth factor receptor 2 in endometrial cancer cells induces cell death despite PTEN abrogation. Cancer Research **2008**;68:6902-7.
13. Gozgit JM, Squillace RM, Wongchenko MJ, Miller D, Wardwell S, Mohemmad Q, et al. Combined targeting of FGFR2 and mTOR by ponatinib and ridaforolimus results in synergistic antitumor activity in FGFR2 mutant endometrial cancer models. Cancer Chemotherapy and Pharmacology **2013**;71:1315-23.
14. Kim DH, Kwak Y, Kim ND, Sim T. Antitumor effects and molecular mechanisms of ponatinib on endometrial cancer cells harboring activating FGFR2 mutations. Cancer Biology & Therapy **2016**;17:65-78.
15. Konecny GE, Kolarova T, O'Brien NA, Winterhoff B, Yang G, Qi J, et al. Activity of the fibroblast growth factor receptor inhibitors dovitinib (TKI258) and NVP-BGJ398 in human endometrial cancer cells. Molecular Cancer Therapeutics **2013**;12:632-42.
16. Kwak Y, Cho H, Hur W, Sim T. Antitumor Effects and Mechanisms of AZD4547 on FGFR2-Deregulated Endometrial Cancer Cells. Molecular cancer therapeutics **2015**;14:2292-302.
17. Weigelt B, Warne PH, Lambros MB, Reis-Filho JS, Downward J. PI3K pathway dependencies in endometrioid endometrial cancer cell lines. Clinical Cancer Research **2013**;19:3533-44.
18. Rodon J, Dienstmann R, Serra V, Tabernero J. Development of PI3K inhibitors: lessons learned from early clinical trials. Nature Reviews: Clinical Oncology **2013**;10:143-53.
19. Yap TA, Bjerke L, Clarke PA, Workman P. Drugging PI3K in cancer: refining targets and therapeutic strategies. Current Opinion in Pharmacology **2015**;23:98-107.
20. Brachmann SM, Kleylein-Sohn J, Gaulis S, Kauffmann A, Blommers MJ, Kazic-Legueux M, et al. Characterization of the mechanism of action of the pan class I PI3K inhibitor NVP-

BKM120 across a broad range of concentrations. Molecular Cancer Therapeutics **2012**;11:1747-57.
21. Chou T, Talalay P. Quantitative analysis of dose-effect relationships: the combined effects of multiple drugs or enzyme inhibitors. Adv Enzyme Regul **1984**:27-55.
22. Sequist L, Cassier P, Varga A, Tabernero J, Schellens J, Delord J-P. Phase I study of BGJ398, a selective pan-FGFR inhibitor in genetically preselected advanced solid tumors. Cancer Research **2014**;74:CT326-6.
23. Sarker D, Ang JE, Baird R, Kristeleit R, Shah K, Moreno V, et al. First-in-human phase I study of pictilisib (GDC-0941), a potent pan-class I phosphatidylinositol-3-kinase (PI3K) inhibitor, in patients with advanced solid tumors. Clinical Cancer Research **2015**;21:77-86.
24. De Buck SS, Jakab A Fau - Boehm M, Boehm M Fau - Bootle D, Bootle D Fau - Juric D, Juric D Fau - Quadt C, Quadt C Fau - Goggin TK, et al. Population pharmacokinetics and pharmacodynamics of BYL719, a phosphoinositide 3-kinase antagonist, in adult patients with advanced solid malignancies. Br J Clin Pharmacol **2014**;78:543-55.
25. Rodon J, Brana I, Siu LL, De Jonge MJ, Homji N, Mills D, et al. Phase I dose-escalation and -expansion study of buparlisib (BKM120), an oral pan-Class I PI3K inhibitor, in patients with advanced solid tumors. Investigational New Drugs **2014**;32:670-81.
26. Guagnano V, Kauffmann A, Wohrle S, Stamm C, Ito M, Barys L, et al. FGFR genetic alterations predict for sensitivity to NVP-BGJ398, a selective pan-FGFR inhibitor. Cancer Discovery **2012**;2:1118-33.
27. Bregar AJ, Growdon WB. Emerging strategies for targeting PI3K in gynecologic cancer. Gynecologic Oncology **2016**;140:333-44.
28. Soria JC, DeBraud F, Bahleda R, Adamo B, Andre F, Dienstmann R, et al. Phase I/IIa study evaluating the safety, efficacy, pharmacokinetics, and pharmacodynamics of lucitanib in advanced solid tumors. Annals of Oncology **2014**;25:2244-51.
29. Pearson A, Smyth E, Babina IS, Herrera-Abreu MT, Tarazona N, Peckitt C, et al. High-Level Clonal FGFR Amplification and Response to FGFR Inhibition in a Translational Clinical Trial. Cancer Discovery **2016**;6:838-51.
30. Konecny GE, Finkler N, Garcia AA, Lorusso D, Lee PS, Rocconi RP, et al. Second-line dovitinib (TKI258) in patients with FGFR2-mutated or FGFR2-non-mutated advanced or metastatic endometrial cancer: a non-randomised, open-label, two-group, two-stage, phase 2 study. The Lancet Oncology **2015**;16:686-94.
31. Klempner SJ, Myers AP, Cantley LC. What a tangled web we weave: emerging resistance mechanisms to inhibition of the phosphoinositide 3-kinase pathway. Cancer Discovery **2013**;3:1345-54.
32. O'Brien C, Wallin JJ, Sampath D, GuhaThakurta D, Savage H, Punnoose EA, et al. Predictive biomarkers of sensitivity to the phosphatidylinositol 3' kinase inhibitor GDC-0941 in breast cancer preclinical models. Clinical Cancer Research **2010**;16:3670-83.
33. Zhong H, Sanchez C, Spitzer D, Plambeck-Suess S, Gibbs J, Hawkins WG, et al. Synergistic effects of concurrent blockade of PI3K and MEK pathways in pancreatic cancer preclinical models. PloS One **2013**;8:e77243.
34. Haagensen EJ, Kyle S, Beale GS, Maxwell RJ, Newell DR. The synergistic interaction of MEK and PI3K inhibitors is modulated by mTOR inhibition. British Journal of Cancer **2012**;106:1386-94.
35. Gozgit JM, Wong MJ, Moran L, Wardwell S, Mohemmad QK, Narasimhan NI, et al. Ponatinib (AP24534), a multitargeted pan-FGFR inhibitor with activity in multiple FGFR-amplified or mutated cancer models. Molecular Cancer Therapeutics **2012**;11:690-9.
36. Chan SL, Wong CH, Lau CP, Zhou Q, Hui CW, Lui VW, et al. Preclinical evaluation of combined TKI-258 and RAD001 in hepatocellular carcinoma. Cancer Chemotherapy and Pharmacology **2013**;71:1417-25.
37. Scheller T, Hellerbrand C, Moser C, Schmidt K, Kroemer A, Brunner SM, et al. mTOR inhibition improves fibroblast growth factor receptor targeting in hepatocellular carcinoma. British Journal of Cancer **2015**;112:841-50.
38. Kotani H, Ebi H, Kitai H, Nanjo S, Kita K, Huynh TG, et al. Co-active receptor tyrosine

kinases mitigate the effect of FGFR inhibitors in FGFR1-amplified lung cancers with low FGFR1 protein expression. Oncogene **2015**; 35:3587-97.

39. Jia S, Liu Z, Zhang S, Liu P, Zhang L, Lee SH, et al. Essential roles of PI(3)K-p110beta in cell growth, metabolism and tumorigenesis. Nature **2008**;454:776-9.
40. Wee S, Wiederschain D Fau - Maira S-M, Maira Sm Fau - Loo A, Loo A Fau - Miller C, Miller C Fau - deBeaumont R, deBeaumont R Fau - Stegmeier F, et al. PTEN-deficient cancers depend on PIK3CB. Proc Natl Acad Sci U S A **2008**;105:13057-62.
41. Edgar KA, Wallin Jj Fau - Berry M, Berry M Fau - Lee LB, Lee Lb Fau - Prior WW, Prior Ww Fau - Sampath D, Sampath D Fau - Friedman LS, et al. Isoform-specific phosphoinositide 3-kinase inhibitors exert distinct effects in solid tumors. Cancer Research **2010**;70:1164-72.
42. Juric D, Castel P, Griffith M, Griffith OL, Won HH, Ellis H, et al. Convergent loss of PTEN leads to clinical resistance to a PI(3)Kalpha inhibitor. Nature **2015**;518:240-4.
43. Schmit F, Utermark T, Zhang S, Wang Q, Von T, Roberts TM, et al. PI3K isoform dependence of PTEN-deficient tumors can be altered by the genetic context. Proc Natl Acad Sci U S A **2014**;111:6395-400.
44. Utermark T, Schmit F, Lee SH, Gao X, Schaffhausen BS, Roberts TM. The phosphatidylinositol 3-kinase (PI3K) isoform dependence of tumor formation is determined by the genetic mode of PI3K pathway activation rather than by tissue type. Journal of Virology **2014**;88:10673-9.
45. Utermark T, Rao T, Cheng H, Wang Q, Lee SH, Wang ZC, et al. The p110alpha and p110beta isoforms of PI3K play divergent roles in mammary gland development and tumorigenesis. Genes & Development **2012**;26:1573-86.
46. Myers AP. New strategies in endometrial cancer: targeting the PI3K/mTOR pathway--the devil is in the details. Clinical cancer research : an official journal of the American Association for Cancer Research **2013**;19:5264-74.
47. Packer LM, Rana S, Hayward R, O'Hare T, Eide CA, Rebocho A, et al. Nilotinib and MEK inhibitors induce synthetic lethality through paradoxical activation of RAF in drug-resistant chronic myeloid leukemia. Cancer Cell **2011**;20:715-27.
48. Carracedo A, Ma L, Teruya-Feldstein J, Rojo F, Salmena L, Alimonti A, et al. Inhibition of mTORC1 leads to MAPK pathway activation through a PI3K-dependent feedback loop in human cancer. The Journal of Clinical Investigation **2008**;118:3065-74.
49. Kinkade CW, Castillo-Martin M, Puzio-Kuter A, Yan J, Foster TH, Gao H, et al. Targeting AKT/mTOR and ERK MAPK signaling inhibits hormone-refractory prostate cancer in a preclinical mouse model. The Journal of Clinical Investigation **2008**;118:3051-64.

Table 1

Inhibitors	Range of concentrations used in IC_{50} calculation	IC_{50} in AN3CA (nM)	IC_{50} in JHUEM2 (nM)	IC_{50} in MFE296 (nM)
BGJ398	0.1 nM– 1 μM	30	20	80
GDC-0941	1 nM - 10 μM	140	355	630
BYL719	1 nM - 10 μM	1730	530	4060
BKM120	1 nM – 10 μM	320	260	695

Figure Legends

Figure 1. Synergistic inhibition of cell viability by combined treatment with BGJ398 and a PI3K inhibitor.

Growth inhibition induced by the FGFR inhibitor BGJ398 and the PI3K inhibitors alone or in combination. AN3CA (A-C), JHUEM2 (D-F) and MFE296 (G-I) cells were treated with the indicated doses of BGJ398, GDC-0941 and BYL719 alone or in combination for 96 hours and an Sulforhodamine B (SRB) assay was subsequently performed. Data are presented as a percentage of the control, in which cells were treated with 0.1% (v/v) DMSO. Points represent the mean of three independent experiments (each performed in triplicate). Error bars represent the standard error of the mean (SEM) and lines were fitted using non-linear regression analysis. Interaction of BGJ398 and GDC-0941 (red circles) or BYL719 (black squares) in AN3CA (C), JHUEM2 (F) and MFE296 (I). Median effect analysis (CalcuSyn software) was used to evaluate the interaction between the inhibitor combinations. Horizontal dotted lines indicate the boundaries for each interaction classification.

Figure 2. Dual targeting of the FGFR and PI3K pathways leads to synergistic inhibition of long-term survival and enhanced cell death.

Clonogenic survival assays in AN3CA (A-B), JHUEM2 (C-D), MFE296 (E-F) treated with the indicated doses (μM) of BGJ398 (BGJ), GDC-0941 (GDC) and BYL719 (BYL) alone or in combination for 72 hours. Cells were then cultured for 16 days without inhibitors and stained with crystal violet. Pictures are representative of three independent experiments. Colonies were counted and expressed as a percentage of the DMSO control. The mean of three independent experiments (each performed in triplicate) for AN3CA (B), JHUEM2 (D) and MFE296 (F) are shown along with the standard deviation (SD). Percentage of apoptotic cells in AN3CA (G), JHUEM2 (H) and MFE296 (I) treated with DMSO, 0.3 μM BGJ398 (BGJ), 0.3 μM GDC-0941 (GDC), 0.6 μM and BYL719 (BYL) alone or in combination for 72 hours. Apoptosis was detected by staining cells with annexin V and propidium iodide. The mean percentage of apoptotic cells from two (JHUEM2) or three (AN3CA, MFE296) independent experiments (each performed in triplicate) is shown along with the SD. Statistical significance between the indicated groups according to a one-way ANOVA is shown (****P<0.0001; ***P<0.001; **P<0.01; *P<0.05).

Figure 3. Inhibition of FGFR and PI3K pathways by BGJ398, GDC-0941 BYL719 and BKM120. AN3CA (A) and JHUEM2 (B) cells were treated for the indicated times with

DMSO, 0.3 μM BGJ398 (BGJ), 0.3 μM GDC-0941 (GDC), 0.6 μM BYL719 (BYL) and 0.6 μM BKM120 (BKM) alone or in combination. Cell lysates were immunoblotted with antibodies for phospho-AKT (Ser473), total AKT, phospho-ERK (Thr202/Tyr204), ERK2, phospho-S6 (Ser240/244), total S6, phospho-4EBP1 (Thr37/46), total 4EBP1, total PARP and cleaved PARP. Tubulin was detected as the loading control. Western blot analysis of AN3CA and JHUEM2 (C) cells transfected with siRNA pools targeting p110α and p110β and a non-targeting (NT) control for 48 hours and treated with 0.3 μM GDC-0941 (GDC) or 0.6 μM BYL719 (BYL) for 6 hours. The mean band intensity of pAKT and pS6 (normalized to tubulin) are shown, along with the SD. The mean level of p110α with p110β knockdown (D) and p110β following p110α knockdown (normalized to tubulin) from three independent experiments along with the SD are also shown.

Figure 4. PI3K inhibition improves anti-tumor efficacy when given in combination with BGJ398. AN3CA (A) and JHUEM2 (B) xenografts were established in nude mice and stratified into six groups (8/group) treated for the indicated number of days with vehicle, 20 mg/kg BGJ398, 75 mg/kg GDC-0941, 12.5 mg/kg BYL719, BGJ398 + GDC-0941 and BGJ398 + BYL719. Mean tumor volumes are shown along with the standard error. Representative tumors including the smallest and largest from each group are shown. C) Tumor growth of AN3CA and JHUEM2 xenografts assessed at 21 days of treatment with inhibitors described in A). Protein lysates from AN3CA (D) xenografts taken from mice treated with the above doses of BGJ398, GDC-0941 or BYL719 for 4 days were lysed and subjected to Western blot analysis for phospho-AKT (Ser473), total AKT, phospho-ERK (Thr202/Tyr204), total ERK, phospho-S6 (Ser240/244), total S6, phospho-4EBP1 (Thr37/46), total 4EBP1. Tubulin was detected as the loading control. E) Immunohistochemical staining of cleaved caspase 3 in AN3CA xenografts treated for 4 days with the indicated drugs, along with the mean of caspase 3 positive cells counted in five fields (x400 magnification) in four tumors (presented as a ratio over vehicle control).

Figure 1

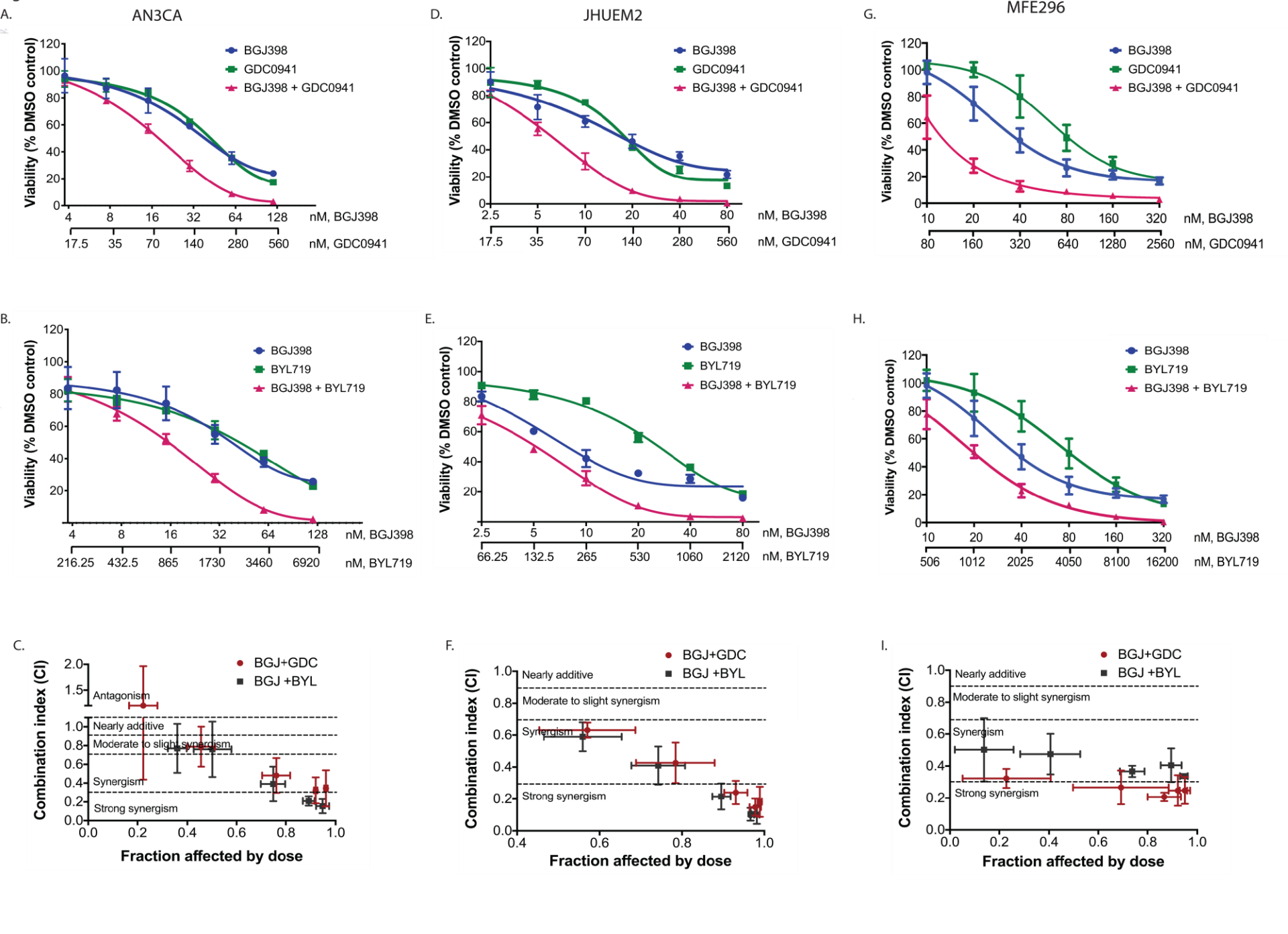
A.
AN3CA
Viability (% DMSO control)
BGJ398
GDC0941
BGJ398 + GDC0941
nM, BGJ398
nM, GDC0941
B.
BYL719
BGJ398 + BYL719
nM, BYL719
C.
BGJ+GDC
BGJ +BYL
Antagonism
Nearly additive
Moderate to slight synergism
Synergism
Strong synergism
Combination index (CI)
Fraction affected by dose
D.
JHUEM2
E.
F.
G.
MFE296
H.
I.

Figure 2

A. AN3CA

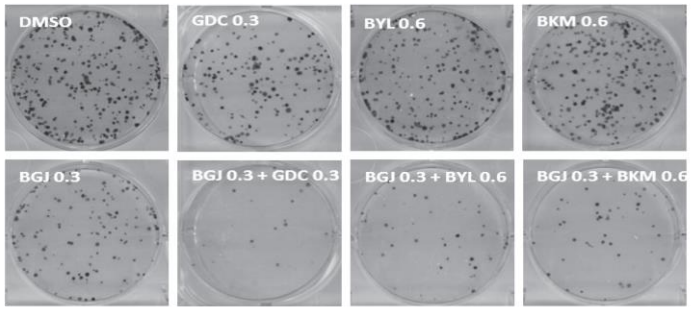

C. JHUEM2

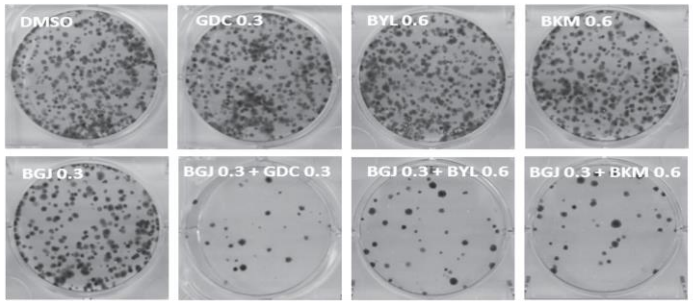

E. MFE296

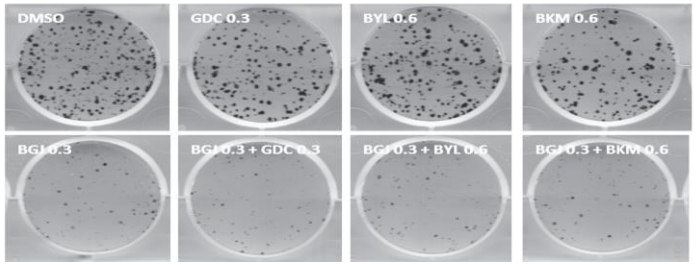

B.

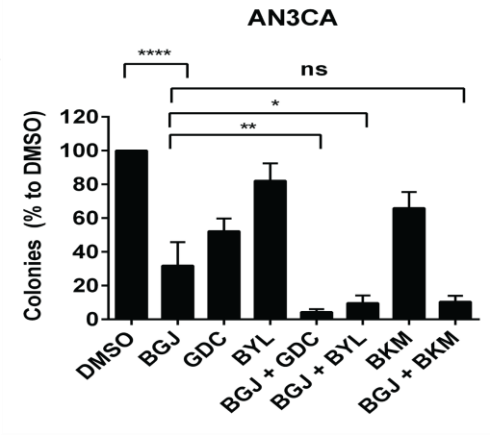

G.

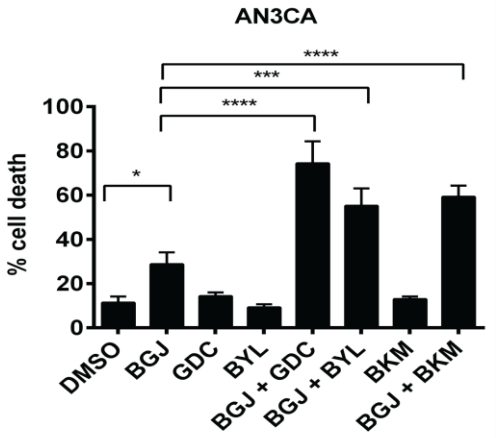

D.

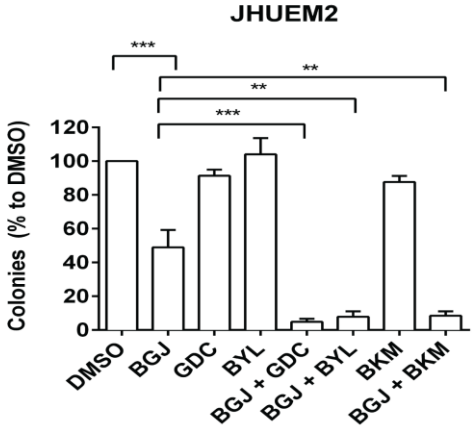

H.

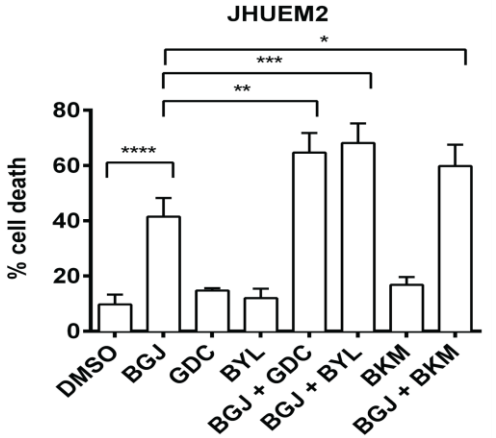

F.

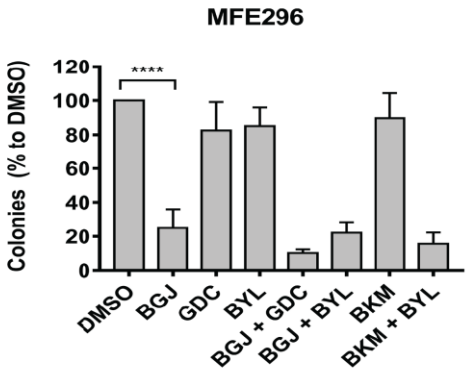

I.

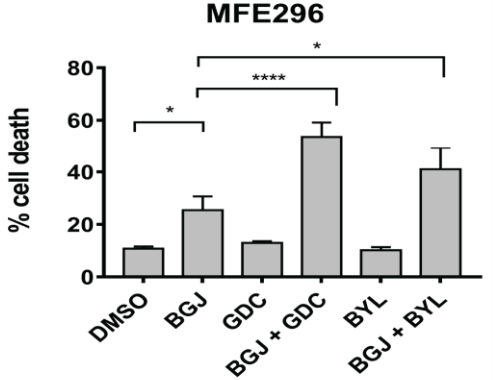

Fig 3.

A. AN3CA

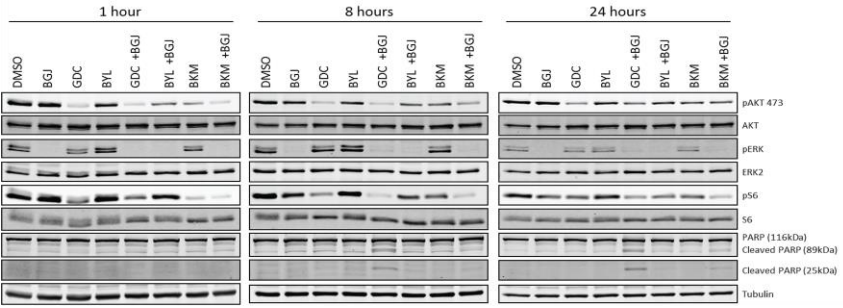

B. JHUEM2

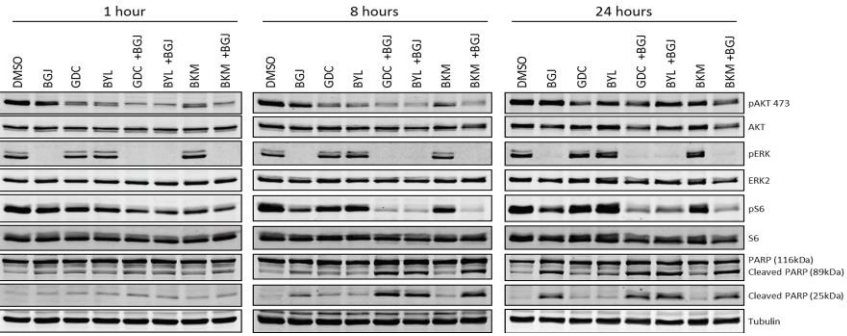

C.

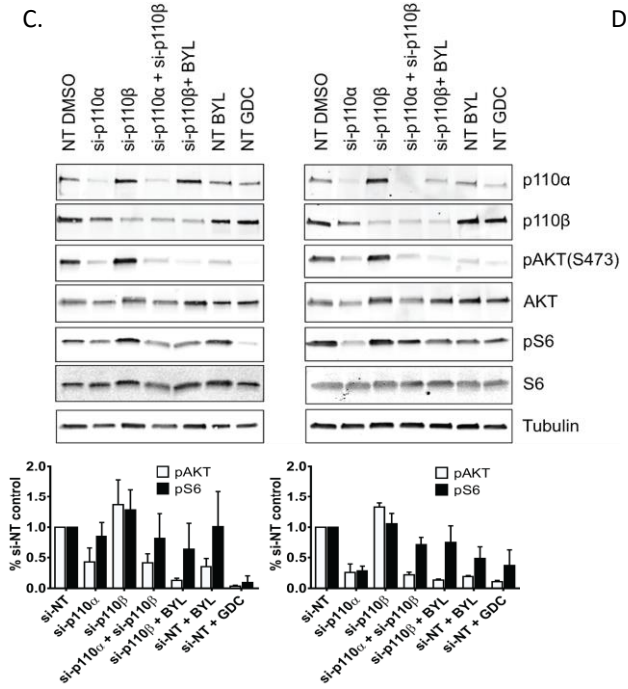

D.

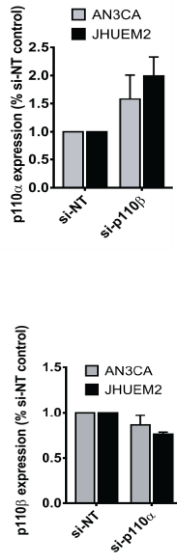

Figure 4

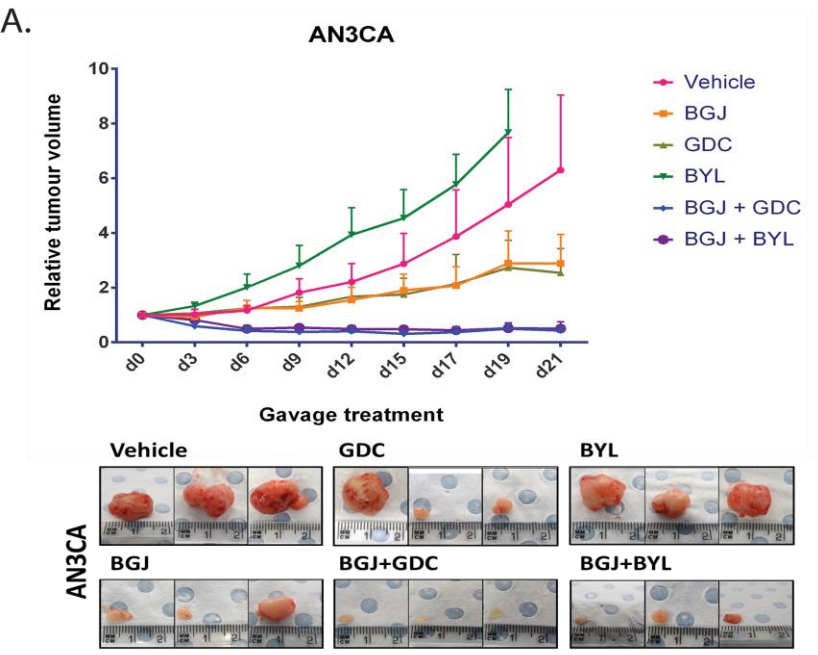
A.
AN3CA
Relative tumour volume
Gavage treatment
Vehicle
BGJ
GDC
BYL
BGJ + GDC
BGJ + BYL
d0
d3
d6
d9
d12
d15
d17
d19
d21
AN3CA
Vehicle
GDC
BYL
BGJ
BGJ+GDC
BGJ+BYL

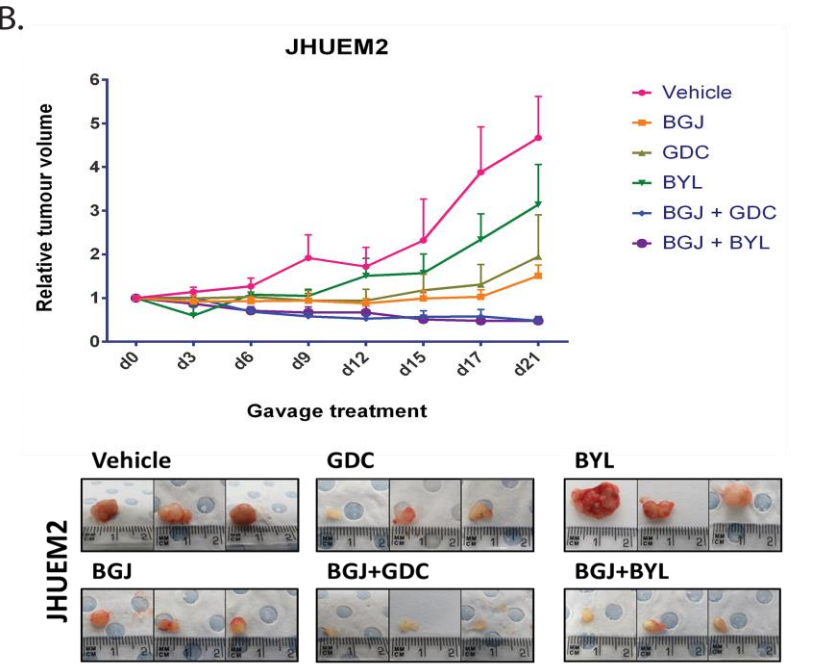
B.
JHUEM2
Relative tumour volume
Gavage treatment
Vehicle
BGJ
GDC
BYL
BGJ + GDC
BGJ + BYL
d0
d3
d6
d9
d12
d15
d17
d21
JHUEM2
Vehicle
GDC
BYL
BGJ
BGJ+GDC
BGJ+BYL

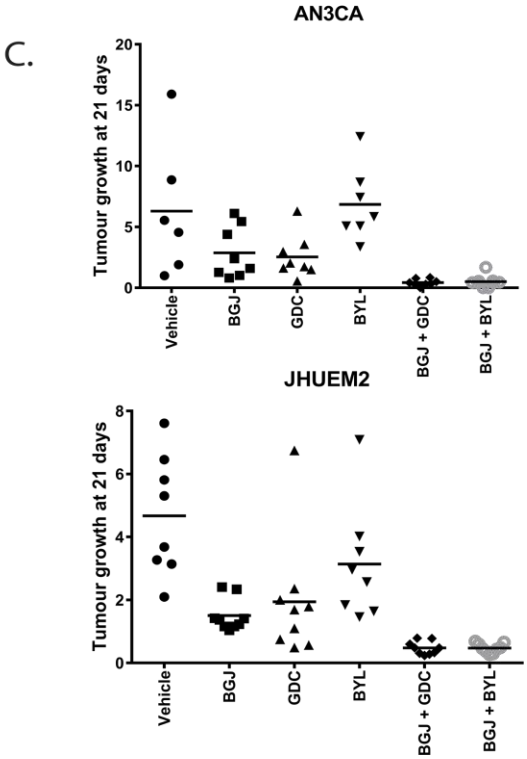
C.
AN3CA
Tumour growth at 21 days
Vehicle
BGJ
GDC
BYL
BGJ + GDC
BGJ + BYL
JHUEM2
Tumour growth at 21 days
Vehicle
BGJ
GDC
BYL
BGJ + GDC
BGJ + BYL

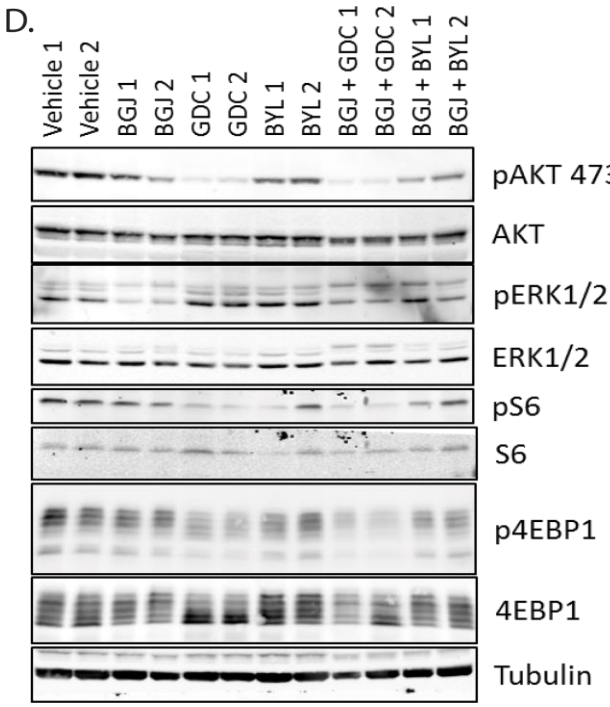
D.
Vehicle 1
Vehicle 2
BGJ 1
BGJ 2
GDC 1
GDC 2
BYL 1
BYL 2
BGJ + GDC 1
BGJ + GDC 2
BGJ + BYL 1
BGJ + BYL 2
pAKT 473
AKT
pERK1/2
ERK1/2
pS6
S6
p4EBP1
4EBP1
Tubulin

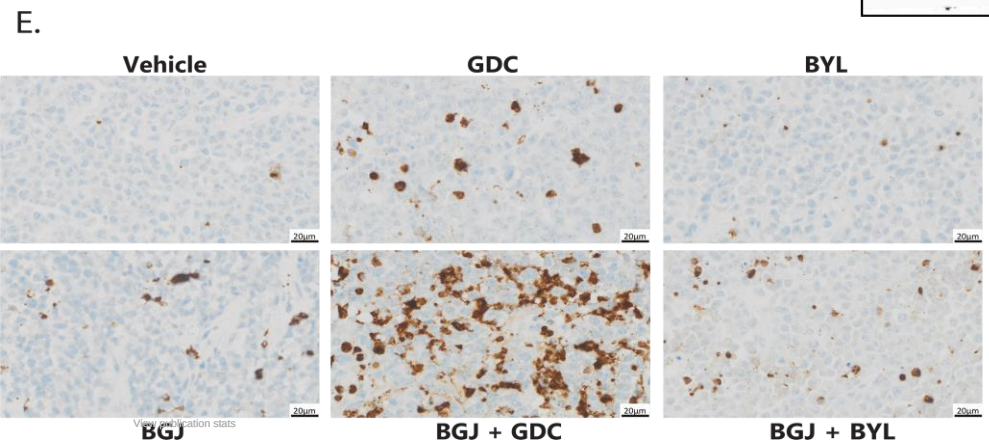
E.
Vehicle
GDC
BYL
BGJ
BGJ + GDC
BGJ + BYL
Caspase 3 positive staining [ratio to vehicle]
Vehicle
BGJ
GDC
BYL
BGJ + GDC
BGJ + BYL